JOURNAL OF MATERIALS SCIENCE **34** (1999) 1791–1798

Transmission electron microscopic investigation of the microstructure of Fe-Cr-Al alloys

R. WITTMANN, S. SPINDLER, B. FISCHER, H. WAGNER, D. GERTHSEN
Laboratorium für Elektronenmikroskopie, Universität Karlsruhe, Kaiserstr. 12, D-76128 Karlsruhe, Germany
E-mail: rolf.wittmann@physik.uni-karlsruhe.de

J. LANGE, M. BREDE
Fraunhofer Institut für Angewandte Materialforschung (IFAM), Lesumer Heerstr. 36, D-28717 Bremen, Germany

J. KLÖWER
Krupp VDM GmbH, Kleffstr. 25, D-58762 Altena, Germany

P. SCHUNK, T. SCHIMMEL
Institut für Angewandte Physik, Universität Karlsruhe, Kaiserstr. 12, D-76128 Karlsruhe, Germany

The microstructure of different Fe-Cr-Al alloys in the composition range of 0 to 18 at % Cr and 7 to 25 at % Al was investigated by transmission electron microscopy (TEM). By systematically varying the compositions, the location of the order-disorder transition was determined. Dark field images confirmed that many samples consisted of a two-phase mixture of small DO_3-ordered particles in a disordered A2 matrix. The mottled contrast exhibited by some samples and sometimes taken as a proof of the existence of ordered particles is shown to be produced by an artefact due to the TEM sample preparation.

1. Introduction

Iron aluminides inspired much interest due to their high resistance with respect to oxidation and sulfidation even at high temperatures, which is coupled with good hot strength and high electrical resistivity [1]. The aluminium oxide surface layers which are responsible for the corrosion resistance are stable at temperatures up to 1000 °C [2]. However, applications have been hampered by the poor cold workability of the material and by the formation of hot cracks during casting which poses severe problems during the industrial production of foils or rods. Substitution of chromium for aluminium improves the mechanical behaviour without significantly reducing the corrosion resistance [3]. Therefore, research has increased on ternary Fe-Al-Cr alloys in recent years (e.g. [4, 5]).

So far, neither the reasons for the improved ductility of the Cr-containing alloys nor the conditions for embrittlement have been clarified. One possible reason could be the existence of an order-disorder transition, ordered phases being suppressed by the introduction of chromium. Around the region of interest, a disordered A2 phase, a partially ordered B2 phase and an ordered DO_3 phase can (co)exist in Fe-Al. Only sparse information is available on the existence regions of the DO_3-phase in the ternary alloys [4, 6]. The investigation of ordered phases in Fe-Cr-Al and of the transitions between them might be of considerable technical importance.

In this study, two systematic series of ternary Fe-Cr-Al alloys are investigated with special regard to the region of existence of the ordered DO_3 phase. For comparison, additional experiments on binary Fe-Al samples are described. Transmission electron microscopy (TEM) is used to determine the microstructure of the specimens, especially with respect to order-disorder phenomena. Special attention will be given to the discussion of the observed contrast phenomena.

2. Experimental procedure

To investigate the order-disorder transition, a series of specimens with constant chromium and varying aluminium content was prepared. The first series consists of specimens with constant chromium content of 17 at % and 15 to 23 at % Al. In the second one, the compositions are varied between 9 at % Cr and 25 at % Al on one side and 18 at % Cr and 8 at % Al on the other. An overview of the compositions of the specimens, together with the results of this investigation, is presented in Fig. 1.

The material was supplied by Krupp VDM GmbH. The alloys were produced by melting the constituents in a vacuum induction furnace, using a zirconia crucible. Ingots of about 10 kg weight were obtained by casting into copper chills. After a solidification period of about 5 h within the crucible, the ingots were air

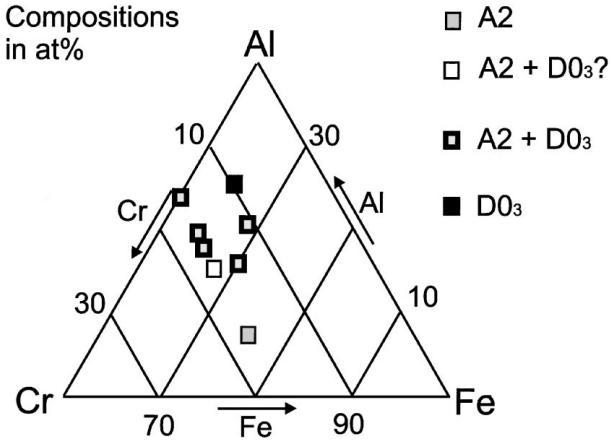

Figure 1 Compositions and resulting microstructure of the investigated specimens.

cooled to room temperature and some small specimens were cut off for wet chemical analysis. At this stage, the material contained a large number of cracks. To destroy the cast structure and homogenize the ingot, samples of the first series were again heated up to 950 °C and rolled, thereby forming sheets of 12 mm thickness. From the hot rolled and as-cast material, respectively, small cylindrical specimens of about 5 mm in diameter were machined and afterwards heat treated as described below.

The elemental components were of standard industrial purity. According to the chemical analysis, the main impurity consisted of 0.25 at % manganese. The compositions of the investigated specimens are listed in Table I. As can be seen, specimens designated by *Pm*/*n* contain approximately *m* at % Cr and *n* at % Al.

The heat treatment for all samples of the first series consisted of annealing at 1000 °C for 5.5 h and air cooling down to room temperature within 2 h. The samples of the second series were investigated in the as-cast state and after annealing for 1 h at 1100 °C and cooling down to room temperature within 12 h. In all these cases, the material thus obtained is not necessarily in thermodynamic equilibrium, which is typical for industrially produced materials.

The TEM specimens were prepared by mechanically cutting disks out of the bulk material, grinding down to a thickness of 100 μm and then polishing electrolytically with 5% perchloric acid and 95% ethanol at a voltage of 40 V and a temperature of −8 °C until perforation. In some cases, the samples were subsequently ion milled for about 1 h with 6 kV argon ions, or electrolytically prepared using a mixture of 1 part HNO_3 in 4 parts ethanol and a voltage of 20 V and a temperature of −15 °C. This last procedure is similar to that applied by Morris *et al*. [7].

TABLE I Chromium and aluminium contents of the specimens of the first (top) and second (bottom) systematic series

Sample	P17/15	P17/18	P17/19	P17/23
Cr [at %]	17.6	16.8	17.6	17.1
Al [at %]	15.1	17.5	18.8	23.4
Sample	P9/25	P11/21	P14/16	P18/8
Cr [at %]	9.3	11.5	13.8	18.0
Al [at %]	25.5	20.8	16.3	7.6

For the room-temperature observations, a Hitachi H700 TEM operated at 200 kV was used. Energy filtered diffraction patterns were taken in a Zeiss EM912Ω TEM operated at 120 kV. In the case of Figs 3 and 4, optimal imaging conditions were obtained by using a cooling stage to reduce the thermal diffuse background, and working with a strongly defocussed beam (the minimal beam aperture of 0.04 mrad) and a long exposure time (300 s).

Heating experiments were performed in an AEI EM7 microscope with a maximum accelerating voltage of 1.2 MV operated at only 400 kV, which was considered to be the optimum compromise between spatial resolution and irradiation damage effects. The temperature accuracy was estimated to be ±20 °C.

Energy dispersive X-ray spectroscopy (EDX) was performed in a Philips CM200 ST/FEG TEM operated at 200 kV and equipped with a Noran Voyager EDX system with germanium detector. A nominal spot size of 2.2 nm was chosen in the nanoprobe mode. To avoid contamination spots during the measurement, a liquid nitrogen cooling stage was used.

Atomic force microscopy (AFM) and lateral force microscopy (LFM) was performed with a commercial instrument (Park Scientific Instruments) and a home-built AFM/LFM head equipped with a beam deflection detection system. Both V-shaped and rectangular silicon nitride cantilevers with pyramidal tips were used. The cantilever force constants for bending were 0.01 and 0.02 N/m, respectively. The torsional force constant of the rectangular cantilever was 8 mN/rad. All AFM/LFM investigations were performed in ambient air and at room temperature. The AFM was operated in the contact mode with a constant total force between tip and sample in the range from 4 to 10 nN.

Throughout the whole article, we will use the indexing scheme of the DO_3 structure for all diffraction patterns, which allows an easier comparison of reflections. (Doing otherwise would result in equivalent reflections for the DO_3 and A2 structures having different indices.) The reflections present in the A2 structure will be called 'matrix reflections', whereas 'superlattice reflections' will designate the additional B2/DO_3 reflections.

3. Results

3.1. Microstructural investigations

After the applied heat treatment, all alloys exhibited an essentially recrystallized structure with a grain size in the order of 0.4 mm for the hot-rolled specimens, and about 3 mm in the other cases. Rarely, some precipitates could be observed. All specimens contained a rather low dislocation density. Only a few, if any, dislocations could be observed in the electron transparent region of the TEM specimens of the constant-chromium series. Therefore, a quantitative determination of the dislocation density could not be accomplished. In the second systematic sample series, the dislocation

density was low, but increasing slightly with increasing chromium and decreasing aluminium content. The dislocation structure of specimens with these compositions will be published elsewhere.

The metastable B32 phase [8] was not observed in any of the samples. Also, an indication of an α-α' demixing or precipitation of the σ-phase could not be found.

3.1.1. Comparison of specimens with constant chromium content: order-disorder transition

The formation of B2 and DO_3 order can be observed by the formation of characteristic superlattice reflections in the diffraction patterns. This can easily be visualized by kinematically simulated diffraction patterns, using the program package EMS [9]. Fig. 2 shows the most important zone axis patterns of the disordered A2 and the ordered B2 and DO_3 phases in comparison. It can be seen that the [111] zone axis is not suitable for a distinction between these phases, because it does not contain any superlattice reflections. From a [100] zone axis pattern, it is not possible to distinguish between B2 and DO_3 order. Best suited are the zone axes [110] and [112], which were used for the following investigations.

The diffraction patterns of sample P17/15 contained matrix reflections, with some very diffuse scattering barely recognizeable near the positions of superlattice reflections (Fig. 3a). With increasing aluminium content, superlattice reflections of the DO_3-type appear. In sample P17/18, they are very faint and diffuse (Fig. 3b), in sample P17/19 they sharpen and increase in intensity (Fig. 3c). In sample P17/23, their intensity and width are comparable to those of the matrix reflections (Fig. 3d).

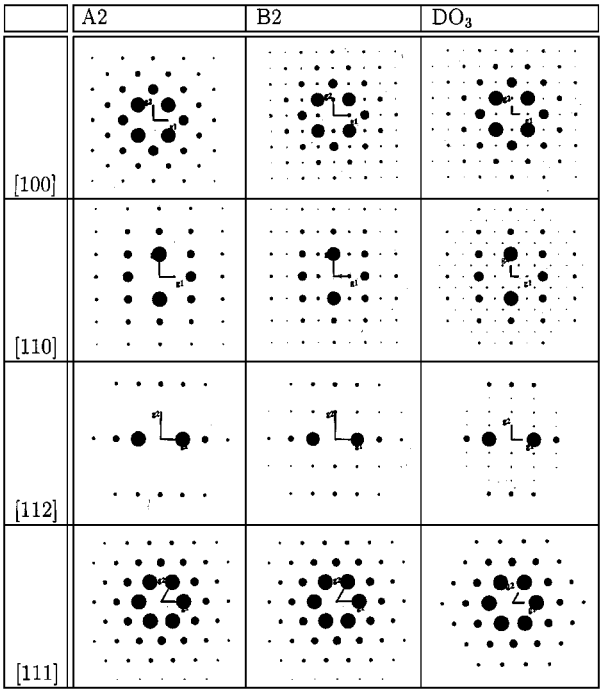

Figure 2 Kinematically simulated diffraction patterns for the zone axes [100], [110], [112] and [111], for the disordered A2 and the ordered B2 and DO_3 phases.

In samples P17/18 and P17/19, the superlattice reflections show a fourfold splitting (Fig. 4) in the [100] zone axis orientation: Instead of one diffuse intensity maximum, four are observed centred around the correct position. Of these four, the one close to the (000) beam is most intense. In less intense diffraction patterns, only this maximum will be seen and misinterpreted as one diffuse superlattice peak shifted from its "correct" position. The splitting amounts to about 10% with respect to the exact position of the 100 reflection in the P17/18 sample and 3% in the case of P17/19.

In the sample P17/23, the intensity of the superlattice reflections allowed dark field images to be taken. Antiphase boundaries were visible, with domain sizes of about 10–20 nm when imaging with a (111)-reflection, and 20–40 nm when using a (222)-reciprocal lattice vector.

3.1.2. Comparison of specimens with 9 to 18 at % Cr and 25 to 8 at % Al: order-disorder transition

The samples of this series were again chosen to contain the order-disorder transition. The intensities of the superlattice reflections increased with decreasing chromium and increasing aluminium content. In sample P9/25, they were very strong, in P11/21 weaker, in P14/16 the superlattice reflections were barely recognizable and showed again a fourfold splitting, and in P18/8 superlattice reflections could not be observed. Comparing the as-cast specimens with those where the additional heat treatment was applied, no difference in the intensity of the superstructure reflections could be recognized.

The P9/25 samples showed a pronounced contrast typical for antiphase boundaries (APBs) [10, 11]. Using B2- and DO_3-type superlattice reflections for dark field imaging, APBs of two different types could be distinguished (Fig. 5). The domain size between the DO_3-type APBs was determined to be about 30–100 nm in the as-cast samples and about three times larger in the samples heat treated at 1100 °C. The APBs which were visible only with B2-type superlattice reflections formed domains with extensions between 0.6 and 3 μm and between 1.5 and 5 μm, respectively.

As the superlattice reflections in the P11/21 samples still remained strong enough, dark field images were obtained with them. By this, the size of the DO_3 particles embedded in a disordered A2 matrix was shown to be about 15–20 nm.

The results of the microstructural investigations are summarized in Fig. 1 and Table II.

3.2. Mottled contrast

In the samples prepared electrolytically with perchloric acid, both bright and dark field images taken under two-beam imaging conditions with matrix reflections revealed a mottled contrast in all samples where superlattice reflections could be observed. A typical example is shown in Fig. 6 where the contrast behaviour

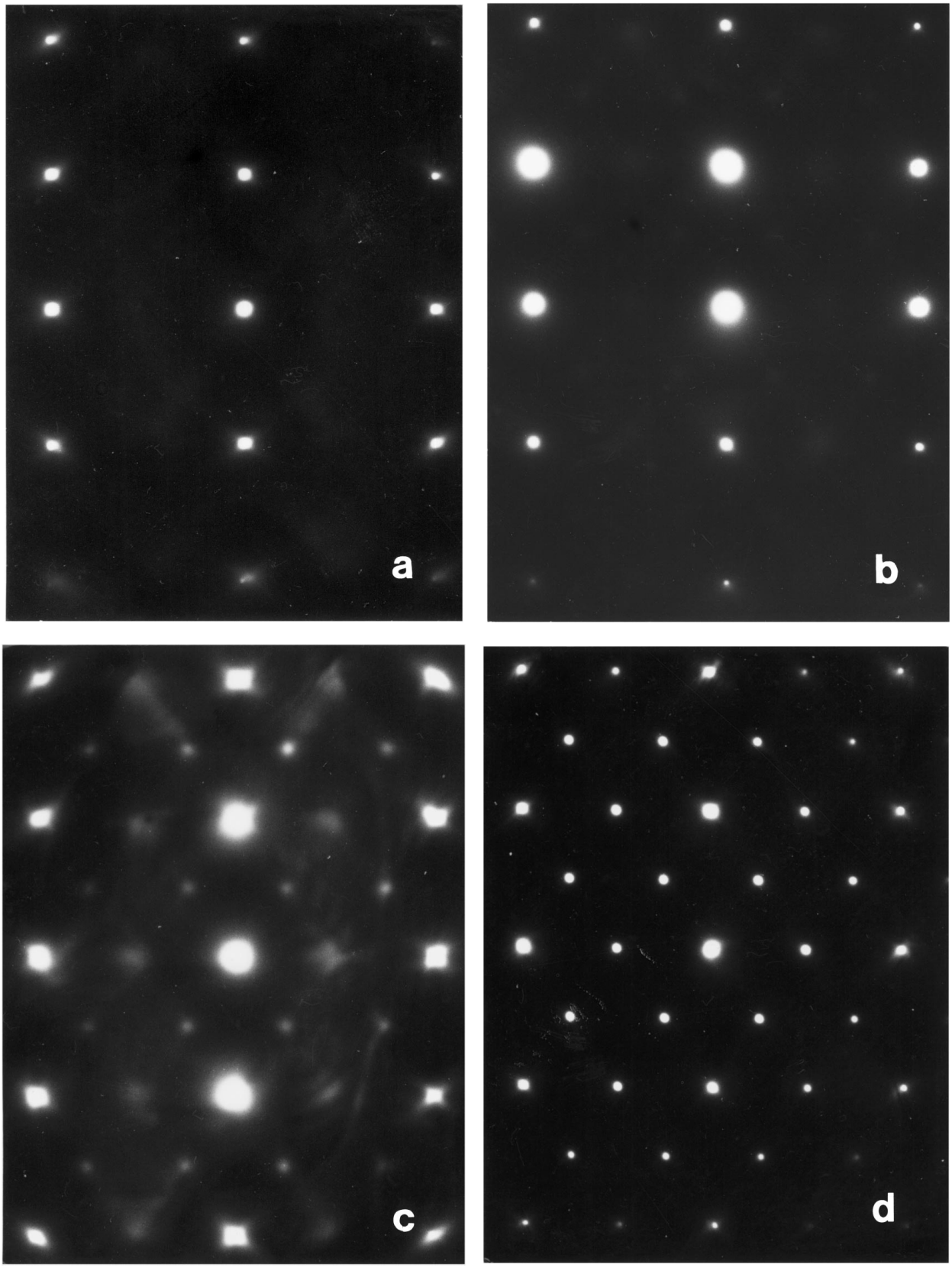

Figure 3 Development of superlattice reflections in zone axis [110]: (a) The basic A2 reflections are observed in sample P17/15. Some extremely weak superstructure reflections are barely visible. (b) Very weak and diffuse peaks appearing at the positions of the DO_3 superstructure reflections in P17/18. (c) Diffuse, but clearly visible DO_3 reflections in P17/19. (d) Pronounced and sharp DO_3 reflections in P17/23, with an intensity of the superstructure reflections almost comparable to that of the matrix reflections. For better comparison, all shown diffraction patterns were recorded with the Zeiss EM912 Omega using its energy filter.

changes around an extinction contour: In bright field images, bright spots are seen on a dark background at the thinner side of the specimen, whereas on the thicker side, dark spots appear against a bright background. In the case of dark field images, the contrast inverses exactly. The average size of the speckles increases with increasing Al content from less than 20 nm in P17/18 to 30–60 nm in P17/23.

TABLE II Summary of the results, indicating the intensity of the superlattice reflections and the microstructure of the specimens. p.o. means partially ordered. DO_3-particle sizes are given where dark field images could be obtained

Sample	Superlattice reflections	Microstructure
P17/15	Barely recognizable	A2 (+DO_3 or B2?)
P17/18	Very weak, diffuse, splitted	A2 + DO_3 (or p.o. DO_3?)
P17/19	Weak, sharp	A2 + DO_3 (or p.o. DO_3?)
P17/23	Strong, sharp	A2 + DO_3-particles with 10–20 nm
P18/8	None	Single-phase A2
P14/16	Very weak, diffuse, splitted	A2 + DO_3 (or p.o. DO_3?)
P11/21	Weak, sharp	A2 + DO_3-particles with 15–20 nm
P9/25	Strong, sharp	Single-phase DO_3

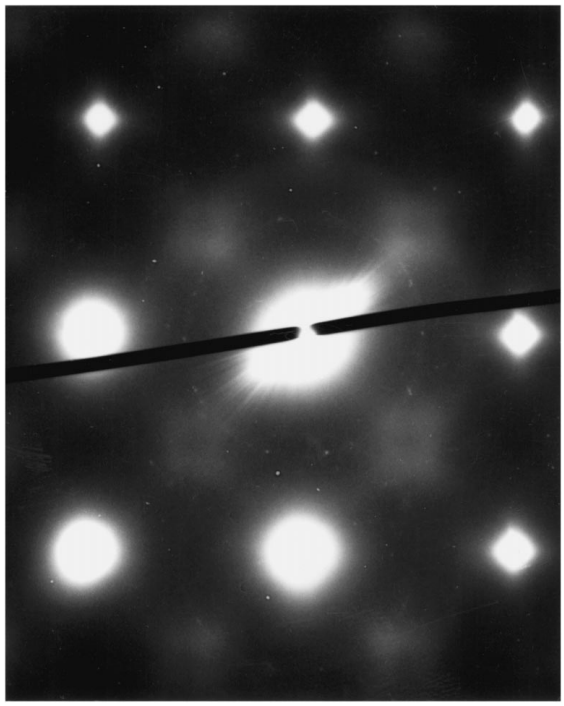

Figure 4 Diffuse superlattice reflection in the [100] zone axis of sample P17/18, as observed in the Zeiss EM912 Omega TEM. A fourfold splitting of the diffuse superlattice peak can be observed.

When preparing the specimens with nitric acid, the mottled contrast could not be observed. Furthermore, additional ion milling of the samples prepared with perchloric acid also removed the contrast.

In-situ heating experiments were performed on samples exhibiting the mottled contrast. On heating up to 550 °C, the superstructure reflections disappeared, proving that the temperature was higher than the ordering temperature. However, the mottled contrast persisted and did not change even after prolonged heating of up to 1 h.

In addition, a P17/23 TEM sample electrolytically prepared with the perchloric acid etchant was investigated by combined atomic force microscopy and lateral force microscopy. Fig. 7 is a typical topographic AFM image of a 800 × 800 nm scanning area, showing a corrugated surface structure containing small pits. The image was obtained with a rectangular cantilever at a total normal force of 4.5 nN between tip and sample. The average roughness was determined as 1.2 nm, while the

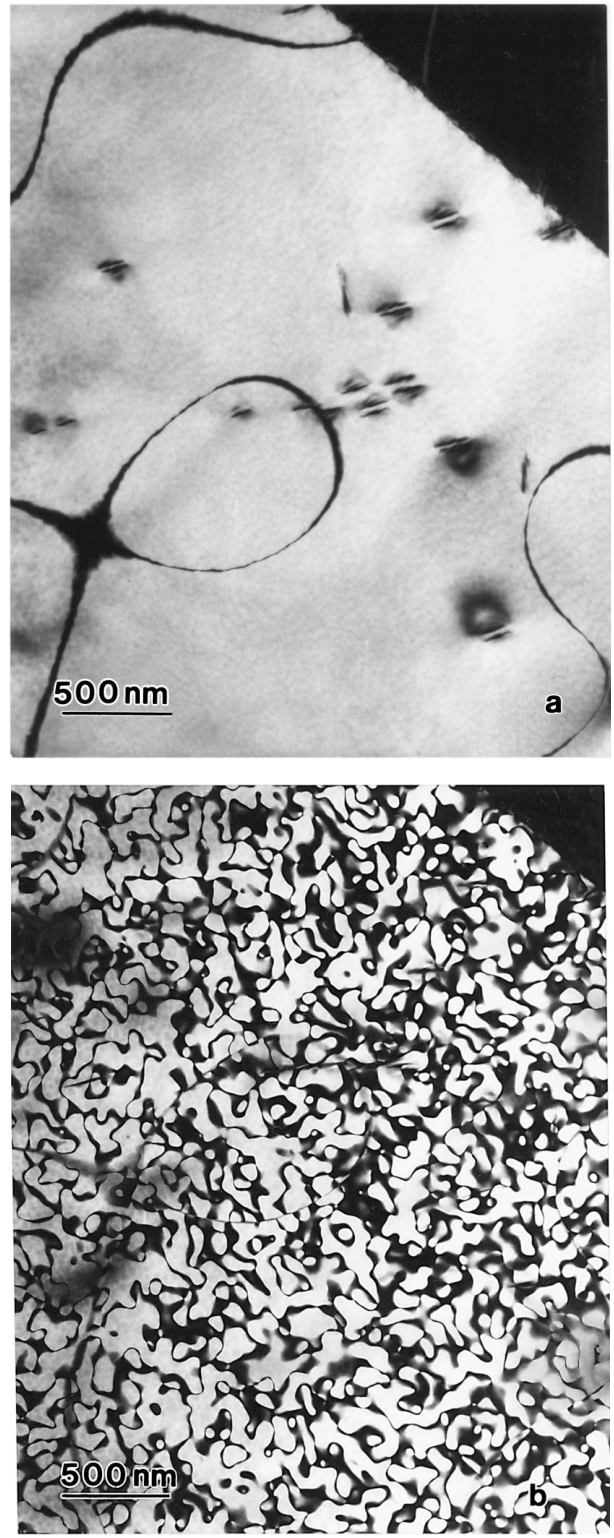

Figure 5 Dark field images of an annealed P9/25 sample obtained in a [011] zone axis (a) with a (200) reflection existing both in the B2 and DO_3 phase, and (b) with a (3 $\bar{1}$ 1) reflection characteristic for the DO_3 phase. In the second image, only antiphase boundaries (APBs) of the DO_3-type are visible, whereas in the first case, APBs of the B2-type with much larger domain size dominate.

corresponding root mean square roughness value was 1.5 nm in the case of Fig. 7. Similar values were found for all images obtained on this sample. Typical pits had a diameter of 30 ± 5 nm and a depth of 2.3 ± 0.5 nm. Simultaneously recorded lateral force images gave no indication of a material contrast between different areas of the surface.

Figure 6 Bright field image with imaging vector $\vec{g} = (220)$ showing a typical example for the mottled contrast behaviour. On the side of the extinction contour closer to the specimen hole, bright spots appear on a dark background, whereas on the thicker side dark spots are superposed to a bright background.

3.3. Further investigations

EDX measurements of the composition were performed on samples P10/19 which consists of a two-phase mixture of DO_3-particles in a disordered A2 matrix. Compositional fluctuations could not be observed within the experimental accuracy of ± 1 at %. On the other hand, the values measured by EDX were in accordance with those measured by chemical analysis within the error bars.

Sometimes, additional reflections were observed which could be attributed to surface oxidation [12].

4. Discussion

4.1. Microstructure

Up to now, ternary phase diagrams do not exist for temperatures low enough to include the DO_3 phase [6]. Only sparse information concerning the DO_3 ordering of ternary Fe-Cr-Al alloys is known at all, besides the general fact that alloying of Cr into Fe_3Al quickly suppresses the formation of ordered phases. Prakash *et al*. [4] systematically investigated the influence of the composition on ordering in ternary Fe-Cr-Al alloys. They proposed that the transition from A2 to DO_3 occurs at a composition of 17 at % Cr and 18.5 at % Al. The investigations of our samples P17/15 and P17/18 show this transition to occur at lower Al contents—close to 15.1 at % Al. This discrepancy could be due to the fact that Prakash *et al*. used X-ray diffractometry for their investigation, which might be less sensitive to discover superstructure peaks of very small intensity (cf. Figs 3 and 4). Another reason could be the different heat treatments applied. It should be noted that none of these heat treatments is suitable to obtain the thermal equilibrium case. Instead, in our case it was chosen to mimick a technologically reasonable temperature curve during production.

Unfortunately, information about the microstructure was not given by Prakash *et al*. [4], besides the claim that all samples were single phase. This seems to be a difference to our observations, where, at least in the cases where superlattice reflections were strong enough to obtain dark-field images, a fine grained two-phase

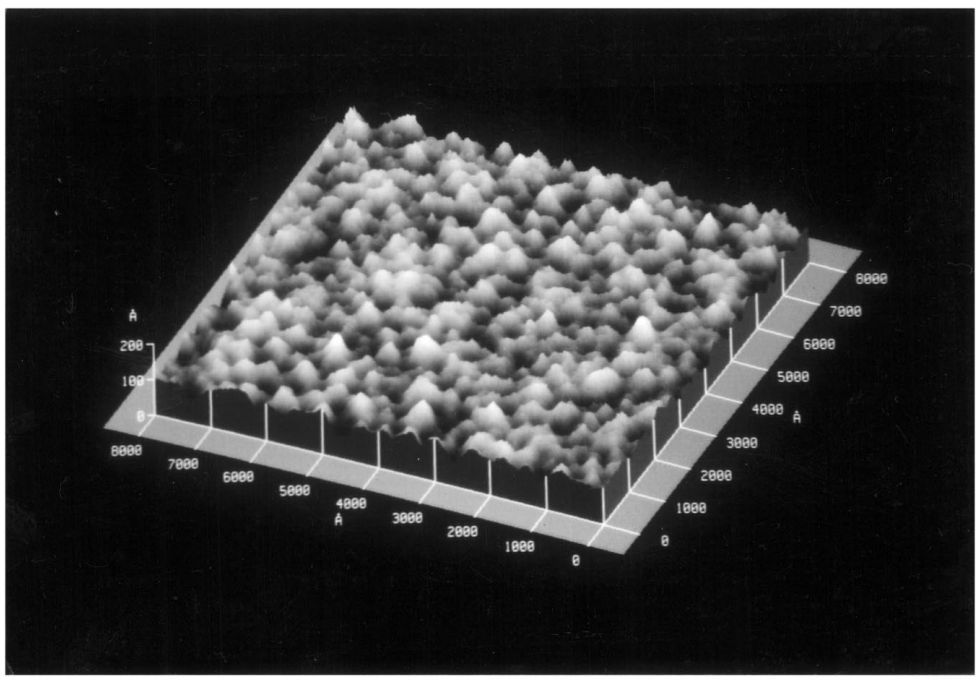

Figure 7 Atomic force microscope image of the surface of a P17/23 TEM specimen electrolytically prepared with perchloric acid (scanning area: 800 × 800 nm). Pits are clearly discernible.

structure of ordered particles embedded in a disordered A2 matrix was recognized. In the specimens with very weak superlattice reflections, however, it has to be left open whether the ordering is due to small fractions of particles or to an partial but homogeneous ordering of the specimens. In binary Fe-Al alloys, the ordering reaction was reported [13, 14] to begin with the transformation of virtually all disordered material into an (imperfectly) ordered DO_3 phase of the same composition. Subsequently, phase separation occurred, with the DO_3 and A2 phase attaining both their equilibrium values for composition and volume fraction.

In the case of the sample P17/15, the superlattice reflections were so weak and diffuse that any definite distinction between B2 and DO_3 was not possible. However, the samples with slightly higher Al content clearly exhibited DO_3-type reflections. What cannot be excluded from the observations is the existence of some residual B2 phase in the specimens in the case of weak intensities of the superlattice reflections. On the other hand, in a study of a binary Fe 24 at % Al alloy [15], the the B2 phase was observed to transform into the DO_3 phase within minutes. As our samples were only slowly cooled, we can assume this transition to be completed. The interpretation in terms of a two-phase mixture of A2 and DO_3 phases is also in accordance with other investigations on binary Fe-Al alloys [14, 16].

Usually, the B32 FeAl phase is considered to be metastable [8]. Only recently, Becker and Schweika [17] concluded the B32 phase to be stable in binary FeAl alloys with about 20 at % Al and proposed an altered version of the standard binary phase diagram of Massalski [18]. In our specimens, the B32 phase was not detected, and therefore these findings cannot be confirmed.

The formation of the σ-phase [19] could not be observed. We also did not find an indication of a chromium-rich α'-phase. It was already pointed out [20] that such a α-α' demixing can be obtained only after extremely long annealing times which are not accessible in usual experiments.

In Cu_3Au, a fourfold splitting of the diffuse superlattice reflections was observed and attributed to correlations between different ordered microdomains embedded in a disordered matrix [21]. A similar mechanism could be a possible explanation of the splitting observed in our case, which would be an indication that these specimens also consist of a two-phase mixture.

4.2. TEM contrast

It is tempting to consider what was called here "mottled contrast" as a proof for a two-phase mixture of tiny ordered particles in a disordered matrix. This is done frequently in the literature [22–24] and discussed in the framework of the dispersed-order model [25]. The contrast is usually attributed to coherency strain due to slightly different lattice constants of particle and matrix predicted by the dispersed-order model. Alternatively, the contrast could be due to differences in extinction length between particle and matrix [26] produced by differences in composition.

The increase in size of the observed speckles with the intensity of the superlattice reflections would be an argument in favour of this dispersed-order conjecture. Also, for high intensities of the superlattice reflections, the existence of ordered particles in a disordered matrix has been confirmed in the case of the P11/21 and P17/23 alloys.

However, the experiments clearly show the mottled contrast to be a preparational artefact of the perchloric acid etchant which could be removed by subsequent ion milling. Using nitric acid for the electrolytic preparation, these artefacts could be avoided. Compositional variations could not be detected between speckles and matrix. Heating experiments showed no dissolution of the presumed particles above the ordering temperature. Instead, the mottled contrast is due to local thickness variations of the TEM foil whose contrast can be observed under dynamic imaging conditions. From the asymmetry of the contrast, it can be deduced that the speckles are due to pits and not to tips. This is confirmed by AFM. The size of the speckles as observed by TEM of approximately 30 nm is in good agreement with the size of the pits observed by AFM (30 ± 5 nm).

The reasons for the development of these pits during electrolytic preparation have to be left open. It cannot be excluded that ordered particles play a role in their formation. This would point to some residual order left in some samples which is not strong enough to produce recognizable superlattice reflections.

5. Summary

Two series of Fe-Cr-Al alloys with systematically varied compositions were investigated by TEM, one with constant chromium content of 17 at % and aluminium contents between 15 and 23 at %, the second with Cr contents between 9 and 18 at % and Al contents between 25 and 8 at %. Both series showed a order-disorder transition to take place. After the applied heat treatments, most samples consisted of a two-phase mixture of DO_3-ordered particles of small size embedded in a disordered A2 matrix. The particle sizes of the ordered phase were determined. The mottled contrast of the samples prepared electrolytically with perchloric acid was shown to be an artefact of the preparation process.

Acknowledgements

We gratefully thank Dr. F. Phillipp, H.-J. Schedler, W. Send and M. Fotouhi for their assistance. The financial support by Deutsche Forschungsgemeinschaft and Bundesministerium für Bildung, Wissenschaft, Forschung und Technologie is gratefully acknowledged.

References

1. C. G. MCKAMEY, J. H. DEVAN, P. F. TORTORELLI and V. K. SIKKA, *J. Mater. Res.* **6** (1991) 1779–1805.
2. H. W. GRUENLING, S. LEISTIKOW, A. RAHMEL and F. SCHUBERT, in "Aufbau von Oxidschichten auf Hochtemperatur-

werkstoffen und ihre technische Bedeutung," edited by A. Rahmel (Deutsche Gesellschaft für Metallkunde, Oberursel, 1992) pp. 7–32.
3. A. AGARWAL, M. J. AKHTAR and R. BALASUBRAMANIAM, *J. Mater. Sci. Lett*. **31** (1996) 5207–5213.
4. U. PRAKASH, R. A. BUCKLEY, H. JONES and G. W. GREENWOOD, *Phil. Mag. A* **65** (1992) 1407–1418.
5. J. A. JIMENEZ and G. FROMMEYER, *Mater. Sci. Eng. A* **220** (1996) 93–99.
6. G. GHOSH, in "Ternary Alloys. A Comprehensive Compendium of Evaluated Constitutional Data and Phase Diagrams Vol. 4: Al-Cd-Ce to Al-Cu-Ru," edited by G. Petzow and G. Effenberg (VCH Verlagsgesellschaft, Weinheim, 1991) pp. 324–343.
7. D. G. MORRIS, D. PEGUIRON and M. NAZMY, *Phil. Mag. A* **71** (1995) 441–463.
8. Z. Q. GAO and B. FULTZ, *Phil. Mag. B* **67** (1993) 787–800.
9. P. STADELMANN, *Ultramicroscopy* **21** (1987) 131–145.
10. A. KORNER, *Phil. Mag. Lett*. **72** (1995) 21–31.
11. D. G. MORRIS, M. LEBOEUF, S. GUNTHER and M. NAZMY, *Phil. Mag. A* **70** (1994) 1067–1090.
12. G. THOMAS, "Transmission Electron Microscopy of Materials" (John Wiley, New York, Chichester, Brisbane, Toronto, 1979) p. 109.
13. D. G. MORRIS and S. GUNTHER, *Acta Mater*. **44** (1996) 2847–2859.
14. S. M. ALLEN and J. W. CAHN, *Acta Metall*. **24** (1976) 425–437.
15. S. M. ALLEN, B. PARK, K. F. LUDWIG, JR. and G. B. STEPHENSON, in "Kinetics of Ordering Transformations in Metals," edited by H. Chen and V. K. Vasudevan (The Minerals, Metals & Materials Society, 1992) pp. 279–290.
16. P. R. SWANN, W. R. DUFF and R. M. FISHER, *Metall. Trans*. **3** (1972) 409–419.
17. M. BECKER and W. SCHWEIKA, *Scr. Mater*. **35** (1996) 1259–1264.
18. T. B. MASSALSKI, "Binary Alloy Phase Diagrams," Vol. 1 (American Society for Metals, Metals Park, 1986).
19. H. L. YAKEL, *Acta Cryst. B* **39** (1983) 20–28.
20. S. M. DUBIEL and G. INDEN, *Z. Metallkd*. **78** (1987) 544–549.
21. S. HASHIMOTO, *Acta Cryst. A* **30** (1974) 792–798.
22. A. MARUCCO and B. NATH, *J. Mater. Sci*. **23** (1988) 2107–2114.
23. A. MARUCCO, *Mater. Sci. Eng. A* **189** (1994) 267–276.
24. H. WARLIMONT and G. THOMAS, *Met. Sci. J*. **4** (1970) 47–52.
25. H.-P. AUBAUER, *Acta Metall*. **20** (1972) 165–172.
26. M. F. ASHBY and L. M. BROWN, *Phil. Mag*. **8** (1963) 1649–1676.

Received 29 October 1997
and accepted 9 November 1998